Effect of basal friction on granular column collapse

Yucheng Li*; Deheng Wei; Ningning Zhang; Raul Fuentes

Institute of Geomechanics and Underground Technology, RWTH Aachen University, 52074 Aachen, Germany

*Corresponding author at: Institute of Geotechnical Engineering, RWTH Aachen University, 52074 Aachen, Germany. E-mail address: li@gut.rwth-aachen.de (Yucheng Li)

The collapse behaviour of granular materials is influenced by many factors, such as aspect ratio and inter-particle friction. However, the specific impact of basal to grain friction on column collapse remains poorly understood. In this study, we systematically analyse the effect of basal friction on gravity-driven granular column collapse using a validated smoothed particle hydrodynamics (SPH) model. The results show that such the basal friction coefficient does influence run-out distance, final height, and deposit morphology. To predict the run-out distance, we propose a modified formula that incorporates the basal friction coefficient, considering two extreme cases, i.e., μ = 0 and $+\infty$. Furthermore, the basal friction also exerts an influence on the final height, with higher friction coefficients resulting in greater final heights. As the friction coefficient increases, the aspect ratio corresponding to the maximum final height also increase. However, we observe a convergence of the effect of basal friction on the final height when $\mu > 0.5$. Moreover, the competition mechanism between the initial column aspect ratio and basal friction coefficient reveals two transition zones between the three main deposit regimes (regime I, regime II, and regime III). This implies that the basal friction can influence the deposit regime. Our findings show the clear influence of basal friction on the collapse behaviour of granular materials and therefore should be carefully considered in future studies.

KEYWORDS: Basal friction coefficient, Aspect ratio, Granular column collapse, Smoothed Particle Hydrodynamics, Regime transition

MANUSCRIPT submitted to Physical review Fluids

Authors: Yucheng Li et al.

List of notations

μ	basic friction coefficient
ρ	mass density of granular material
v	Poisson’s ratio
a	aspect ratio
φ	internal friction angle
E	elastic modulus material
g	gravitational acceleration
r_0	initial radius
r_∞	final run-out distance
h_0	initial height
h_∞	final height

I. INTRODUCTION

Granular column testing and studies are a traditional reference experiment to study the failure and rheological behaviour of granular media. Their study is useful in multiple applications such as natural disasters, optimizing industrial processes, and advancing fundamental research in physics and materials science.

Of critical importance for certain applications, such as landslides, is to understand the characteristics of the final deposit run-out, including its final run-out distance, height, and final morphology. Until now, the widely accepted and reported results in the literature indicate that the run-out distance is mostly governed by the initial aspect ratio [1-6]. Fundamental studies by [1], who used five types of grains (different particle sizes and shapes), and [2] who used two types of glass beads (different particles sizes but the same particle shape) propose a bilinear relationship of the same form between initial aspect ratio, a (defined as $a = h_0/r_0$, where h_0 is initial height and r_0 is initial radius), and normalized run-out distance, $R^* = (r_\infty - r_0)/r_0$ (where r_∞ is final run-out distance). The scaling law is of the form $R^* = \alpha \cdot a^\beta$ (where the coefficient α and exponent β are obtained from experimental results) as shown in FIG. 1.

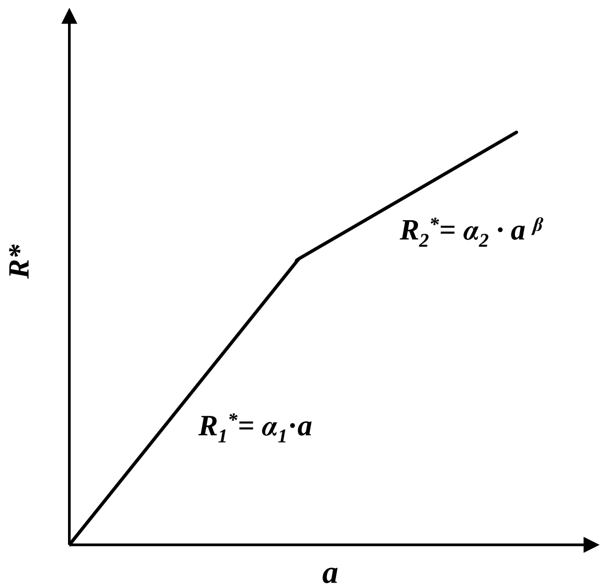

FIG. 1. A sketch of the bilinear relationship between R^* and a (log-log form).

More recent results have shown that the relationship collapses into a single line when also considering the kinematics of the moving front [7]. However, other affecting parameters have been also recently studied. For example, the effects of an erodible surface [8, 9], grain size effects (R_0/d) [10, 11], and collapse in water or cohesive materials collapse [6, 12, 13] have been investigated. Despite these many publications, only a handful of studies are dedicated to the effect of the friction coefficient between the substrate and column grains; herein called basal friction coefficient, μ. This has resulted in an apparent lack of consensus on whether it has an effect and where exactly it is most prominent. Goujon, et al. [14] conducted experiments to study the effect of roughness of the inclined plane on the dynamics of granular flows with different-sizes beads flowing over a plane where a layer of the same beads was glued. It appears from these experiments that the relative roughness, defined as the ratio between the size of flowing beads and the size of glued beads is critical to determine the run-out distance. Contrary to this, Lube, et al. [1] reported that the roughness of the ground made no significant effect on the deposit results. Lajeunesse, et al. [2] found that for columns with larger aspect ratios, roughness had no effect on the final run-out distance, and only had influence on the final height. Roche, et al. [15] generated a column of particles initially fluidized with air to eliminate the inter-particle friction in the granular columns, and concluded that fluidization reduces contacts between the grains and increase the coefficient α ($R^* = \alpha \cdot a^{\beta}$) compared to dry flows but it has no effect on the exponent β. However, fluidized particles also reduce the friction between column grains and run-out plate although they did not analyse this. In numerical studies, Frank [16] used the three-dimensional discrete element method (DEM) to study the effect of the static friction coefficients (μ_s=0.4 and μ_s=0.65) on the collapse of granular column with a fixed aspect ratio of a = 1.91. They discovered that the run-out distance and final deposit height remain unaffected by the static friction coefficient. Zhang, et al. [17] studied the quasi-static collapse of two-dimensional granular columns using particle finite element method (PFEM) simulations. They reported that the change of basal roughness not only significantly influences the collapse process quantitatively, but may lead to new failure patterns that have not been observed in the experiments of quasi-static collapse. Sheikh, et al. [18] proposed two frictional boundary algorithms (penetration method and momentum mothed) of SPH and then test them to investigate the effect of basal friction (μ = 0.0, 0.2, 0.4 and 0.9) on the collapse behaviour of granular columns. Their results show that the flow of a collapsing granular column can be divided into three deposit regimes and the interaction of collapsing regimes is affected by basal friction. Also, their results show that the normalized run-out distance increases as μ decrease and this effect becomes negligible for large aspect ratios. However, they do not have a systematic analysis of μ and do not incorporate it into the formula for predicting run-out distance. Furthermore, with consideration of both inter-particle friction and particle-boundary friction, Man, et al. [19] proposed a dimensionless number, the effective aspect ratio, $\alpha_{eff} = \sqrt{\frac{1}{\mu_w+\beta\mu_p}}\left(\frac{h_0}{r_0}\right)$ (where μ_w is the basal friction coefficient, μ_p is the inter-particle friction coefficient, and β is a fitting parameter) to analysis the deposit morphology of the granular column collapse. However, they did not consider the extreme conditions (zero and +∞) of the particle-boundary friction, which resulted in findings that only show one transition zone between three types of deposit regimes.

Despite this mounting evidence, no study has yet systematically investigated the basal friction coefficient influence on collapse behaviour. Hence, in this study, we use SPH to analyse the effects of basal friction on gravity-driven particle column collapse. By using various basal friction coefficients μ, a modified model for predicting the run-out distance considering μ has been proposed. The model is fully physical consistent as it also considers two extreme cases, i.e., μ = 0 and +∞. Furthermore, the basal friction effect on final height and deposit regime transition were also analysed.

The next section briefly introduces the SPH framework, explains the model construction, and then validates the model against existing experiments. Sec. III presents the results and discussions of the effects of various basal friction coefficients on the deposit results. Finally, Sec. IV concludes this paper.

II. METHODS

A. SPH framework

SPH has been broadly demonstrated for the modelling of large deformation granular materials, including granular column collapse [20-25]. We use the SPH solver in LS-DYNA [26], that uses an explicit code developed for the dynamic analysis of non-linear problems and has the advantage of widely available material models suitable for granular materials.

In SPH the governing equations for the bulk are discretised over a set of particles, each representing a certain volume and therefore with a certain mass obtained from the initial density of the material they represent. Each particle is used to calculate the different variables, such as velocity and stresses (forces) where the continuum is approximated by a summation of quantities for each particle. Hence, a variable (e.g., velocity or stress) can be approximated everywhere using the function:

$$f(\boldsymbol{x}_i) = \sum_{j \in P} w_j f(\boldsymbol{x}_i) W(\boldsymbol{x}_i - \boldsymbol{x}_j, h), \tag{1}$$

where $w_j = \frac{m_j}{\rho_j}$ is the "weight" of the particle, h is the smoothing length which varies in time and space, and $W(\boldsymbol{x}, h)$ is the kernel function. The kernel function is defined using the function θ though the relation:

$$W(\boldsymbol{x}, h) = \frac{1}{h(\boldsymbol{x})^d} \theta(r), \tag{2}$$

where d is the number of space dimensions and $r = \left\|\boldsymbol{x}_i - \boldsymbol{x}_j\right\|/h$. Here, $\theta(r)$ is the cubic B-spline function and defined as

$$\theta(r) = C \begin{cases} 1 - \frac{3}{2}r^2 + \frac{3}{4}r^3, & 0 \leq r \leq 1 \\ \frac{1}{4}(2-r)^3, & 1 \leq r \leq 2 \\ 0, & otherwise \end{cases}, \tag{3}$$

where C is a constant of normalization that depends on the number of the space dimensions.

The great advantage of such formulation is that the discrete form of the gradient operator of a function can be also calculated based on the gradient of the kernel function,

$$\frac{\partial f(\boldsymbol{x}_i)}{\partial \boldsymbol{x}} = \sum_{j\in P} w_j \left(f(\boldsymbol{x}_j) - f(\boldsymbol{x}_i)\right)\nabla W_{ij}, \tag{4}$$

with $\nabla W_{ij} = \frac{\partial W_{ij}}{\partial \boldsymbol{x}_i}$.

Finally, this allows writing partial differential governing equations in a discrete form. For example, the mass conservation in the framework of standard SPH becomes,

$$\frac{d\rho_i}{dt} = -\sum_{j\in P} m_j\left(\boldsymbol{v}_j - \boldsymbol{v}_i\right)\cdot \nabla W_{ij}; \tag{5}$$

and

$$\frac{d\boldsymbol{v}_i}{dt} = \sum_{j\in P} m_j \left(\frac{\boldsymbol{\sigma}_i}{\rho_i^2} + \frac{\boldsymbol{\sigma}_j}{\rho_j^2}\right)\nabla W_{ij} + \boldsymbol{b}_i, \tag{6}$$

where, $\boldsymbol{b}_i$ denotes the external body forces. Artificial viscosity is also implemented and shown in Appendix A. To simulate the failure behaviour of the granular column, we use the Mohr-Coulomb constitutive model,

$$\tau_{max} = C + \sigma_n \cdot \tan\varphi, \tag{7}$$

where $\tau_{\max}$ is maximum shear stress on any plane, σ_{n} is normal stress on that plane, C is a cohesion, and φ is internal friction angle. Since our material is dry, C is zero.

B. Model construction and collapse

A sketch of granular column collapse is shown in FIG. 2(a), where a cylindrical domain discretised by SPH particles is placed over a rigid horizontal surface. The friction force (F_S) between the rigid plane and SPH particles is limited by the friction coefficient, μ, in the dry Coulomb friction model: $F_s = \mu F_N$, where F_N is the normal contact force. μ was initially set to 0.4 in accordance with the validation experiments of [1]. Several relevant papers utilizing SPH simulations have validated these experimental results [1], with their respective material parameters summarized in TABLE .

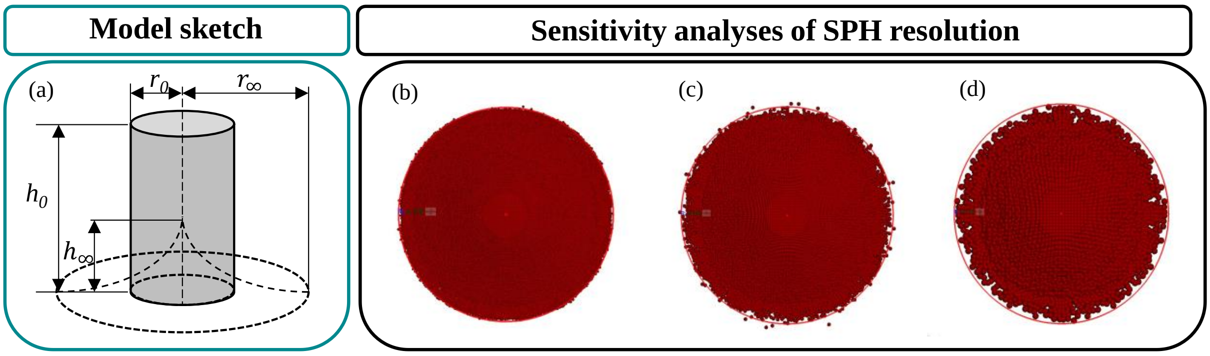

FIG. 2. (a) A sketch of the axisymmetric granular collapse: shaded region denotes the initial column (r_0: initial radius, h_0: initial height), dashed curve denotes deposit geometry (r_∞: final run-out distance, h_∞: final height). (b) Particle spacing: Δp=2.0mm, a=0.55. (c) Δp=3.0mm, a=0.55. (d) Δp=5.0mm, a=0.55.

TABLE I. Material parameters used in previous studies.

Database	*Setup*	ρ/kg.m^{-3} *Density*	*a/-* *Aspect ratio*	φ/° *Angle of friction*	υ/- *Poisson's ratio*	E_i /MPa *Young's modulus*
Ref. [1]	Expt. axisymmetric	2600	0.19-13.8	-	-	-
Ref. [20]	Num. axisymmetric	2600	0.225-20	30	0.3	6
Ref. [21]	Num. axisymmetric	2600	0.25-9.5	30	-	-
Ref. [22]	Num. axisymmetric	2600	0.5-4.0	33/37	0.3	20.16
Ref.[27]	Num. axisymmetric	1570	0.5-11	28	0.3	12
Ref. [28]	Num. axisymmetric	2600	0.5	37	-	-
Ref. [24]	Num. axisymmetric	2600	0.2-30	30	0.3	5.98
This study	Num. axisymmetric	2600	0.4-25	37	0.3	6.00

Prior to conducting the simulation, we performed a sensitivity analysis to determine the optimal number of particles that can balance computational cost and accuracy. Figures 2 (b), 2 (c), and 2 (d) illustrate three final deposit patterns with different particle spacings, Δp (the distance between adjacent particles in the global coordinate of 2.0, 3.0 and 5.0mm), with corresponding SPH particle numbers of 220080, 63378, and 13904, respectively. A red circle with a radius of 0.176 m was used as a standard reference size for better comparisons. We observed similar results for Δp of 2.0 and 3.0mm, while the boundary was discontinuous for Δp = 5.0mm due to the insufficient number of particles. Hence, Δp = 3.0mm was chosen for all simulations in this study.

As summarized in **Error! Reference source not found.**, 18 cases with different granular column aspect ratios covering a wide range from 0.4 to 25 were simulated. Note that in the models only the column height was changed, while the column radius (r_0 = 0.1m) remained constant.

TABLE II. Test series of granular column collapse.

Case ID	$a = h_0/r_0$	h_0 /m	No. of particles
1	0.4	0.04	49,294
2	0.55	0.055	63,378
3	0.7	0.07	84,504

4	0.8	0.08	95,067
5	0.9	0.09	105,630
6	1.0	0.10	119,714
7	1.5	0.15	176,050
8	2.75	0.275	323,932
9	4	0.4	471,814
10	6	0.6	704,200
11	8	0.8	940,107
12	9	0.9	1,056,300
13	10	1.0	1,176,014
14	12	1.2	1,408,400
15	13.8	1.38	1,619,660
16	15	1.5	1,760,500
17	18	1.8	2,112,600
18	25	2.5	2,932,993

C. Initial Validation

To validate whether our SPH can capture the rheological behaviour of granular columns, these results focus on flow patterns, while the run-out distances that also serve as validation will be illustrated in Section. 3. FIG. 3 compares the evolution of the model flow patterns with experimental patterns of three typical aspect ratios from Ref. [1]. The three aspect ratio values induce three clearly different flow patterns and final deposition characteristics. For small aspect ratios (e.g., a = 0.55), the collapse starts from the perimeter and spreads to the interior of the model, maintaining the initial height during the process. After collapse, a flat surface remains at the top of the model. For intermediate aspect ratios (e.g., a = 2.75), the model cannot maintain its initial height during the collapse, and the top surface changes from a flat plate to a conical tip. For large aspect ratios (e.g., a = 13.8), the top surface of the model maintains a flat shape during the collapse until the upper particles reach the static area at the bottom, after which it begins to collapse around the static area, resulting in a transition from a plane to revealing the tip (cusp) of the conical static area. During this process, the sand forms an outward propagating wave that transfers mass from the centre to the edge of the diffusion, forming a concentric wave at the final deposit. Our numerical flow patterns agree well with their experimental results.

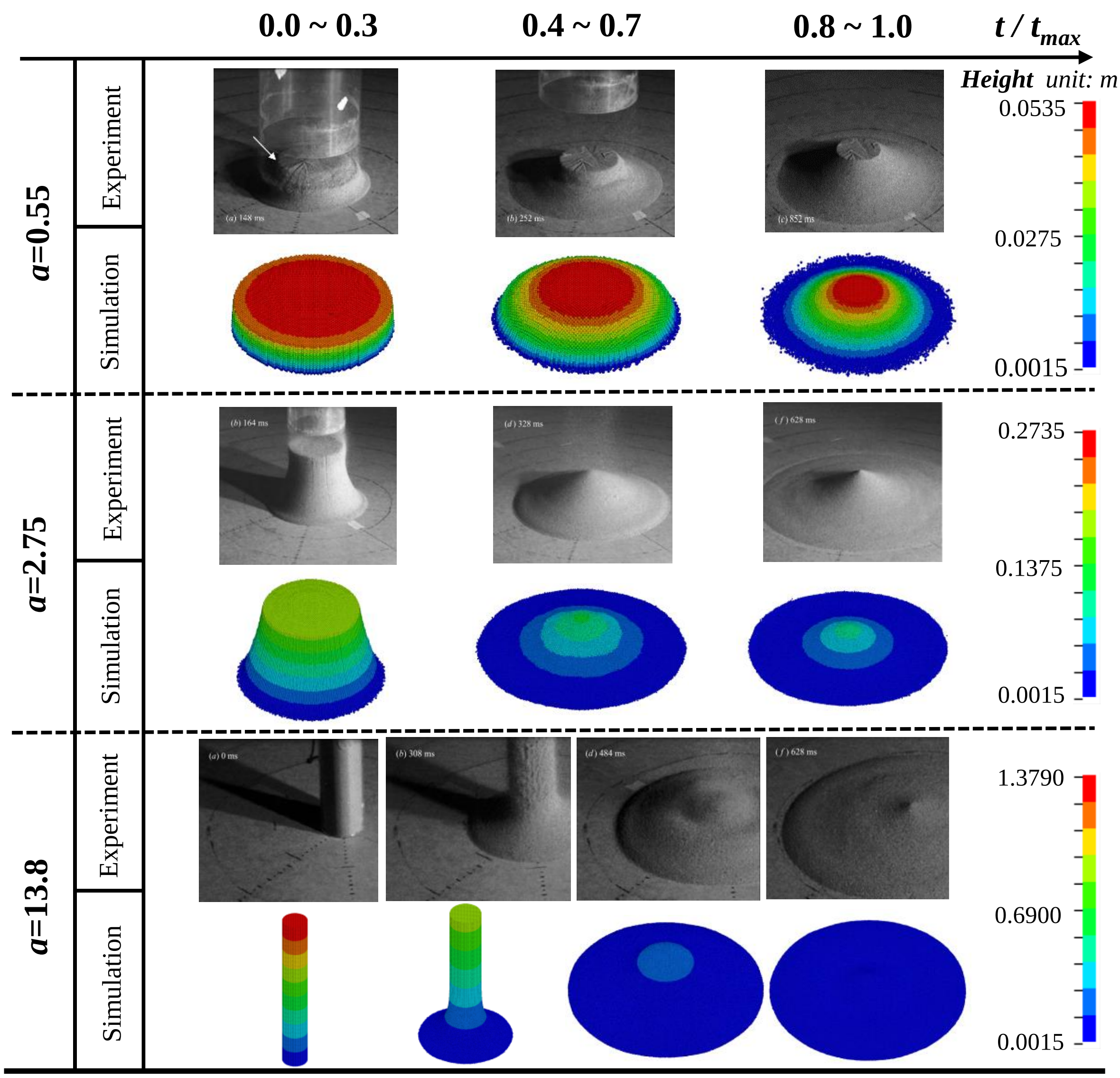

FIG. 3. Granular column collapse evolution at various time points observed in three columns with representative aspect ratios (coloured images with colour bar) and finial experimental collapse patterns reported in Ref. [1] (grey images).

III. RESULTS AND DISCUSSION

Values of the basal friction coefficient (μ) from 0.1 to 1.8 were used to investigate its influences on sand column collapse, including run-out distance, final height, and morphology.

A. Run-out distance

We determine the run-out distance of the granular column using the 'effective' run-out distance method proposed by Ref. [24]. Figure 4 shows a comparison of the normalized run-out distance between simulations and experiments. For μ = 0.4, cited by Ref. [1], the numerical results shows a good agreement with the experimental data, but also are consistent with the other types of simulations [21, 22]. Reported experimental and numerical simulations have indicated a linear relationship between the initial column aspect ratio and the normalized run-out distance (see Fig. 1 and Table III). We investigate further this relationship in light of the evident effect of the friction coefficient μ (see Table IV) for both low and large aspect ratios.

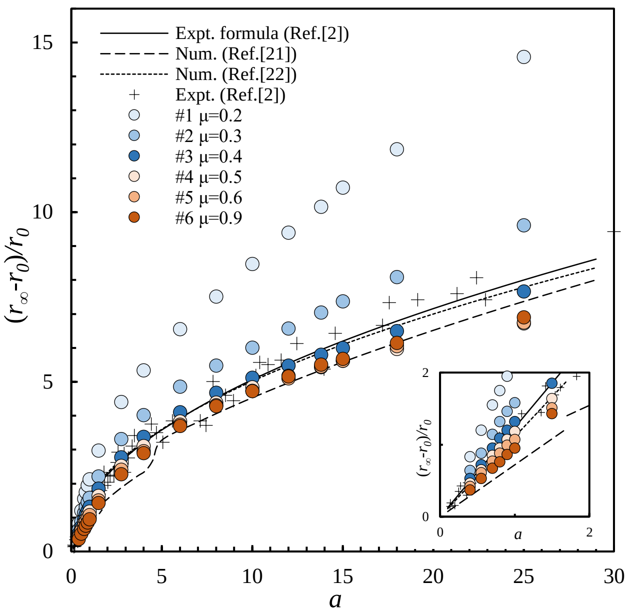

FIG. 4. Comparison of the normalized run-out distance between different simulations and experiments.

TABLE III. Proposed formula for predicting the deposit run-out distance.

Database	Formula form
Expt. axisymmetric**: Ref. [1]**	$R^* = \frac{r_\infty - r_0}{r_0} \simeq \begin{cases} 1.24a, & a < 1.7 \\ 1.6a^{1/2}, & a \geq 1.7 \end{cases}$
Num. axisymmetric**: Ref. [21]**	$R^* \simeq \begin{cases} 0.72a, & a < 1.7 \\ 1.02a^{3/5}, & a \geq 1.7 \end{cases}$
Num. axisymmetric**: Ref. [22]**	$R^* \simeq \begin{cases} 1.11a, & 0 \leq a < 1.7 \\ 1.66a^{0.48}, & a \geq 1.7 \end{cases}$

The inset of Fig. 4 shows that R^* varies linearly with the aspect ratios when $a < 1.7$. Hence, we propose the introduction of μ to R^* by writing

$$R^* = f(\mu) \cdot a, \tag{8}$$

where $f(\mu)$ is an unknown function. To achieve plausible forms of f over the whole range of a, we must make sure that for $\mu = 0$, the collapsed grains would never stop and thus $R^* \to \infty$. Following the same logic, when $\mu \to \infty$, every grain would become quiescent at all times as soon as it touches the substrate, under which the column can be deemed collapsed onto one layer of its composed grains. With these two asymptotic values of $f(\mu)$ in mind, we assume that

$$f(\mu) = \frac{O}{\mu^P} + Q, \tag{9}$$

where O, P, and Q are fitted parameters and are all positive.

This form of f, satisfies that for increases of μ, the difference between slope between R^* and a gradually vanishes (see Fig. 5(a)). When μ approaches to zero, the particles are not limited in the horizontal surface, and when μ is infinity, the bottom layer particles are fixed to the substrate, and other particles slide on the bottom layer particles. The fitting curve to the numerical simulations in FIG. 5(b) gives values of "$O = 0.1834, P = 1.268, Q = 0.7536$" with a high R^2 value of 0.998. The fact that $f(\mu)$ approaches to 0.7536 when $\mu \to \infty$, means that the minimum run-out distance for a given μ increases linearly as the aspect ratio increases, with a slope of 0.7536. Somewhat surprisingly, this value is equal to the tangent value of the internal friction angle (tan 37°=0.7536) of the material. This would indicate that the minimum run-out distance depends on the material internal friction angle. Using the fitted values, the proposed formula is:

$$R^* = \left(\frac{0.1834}{\mu^{1.268}} + 0.7536\right) \cdot a \tag{10}$$

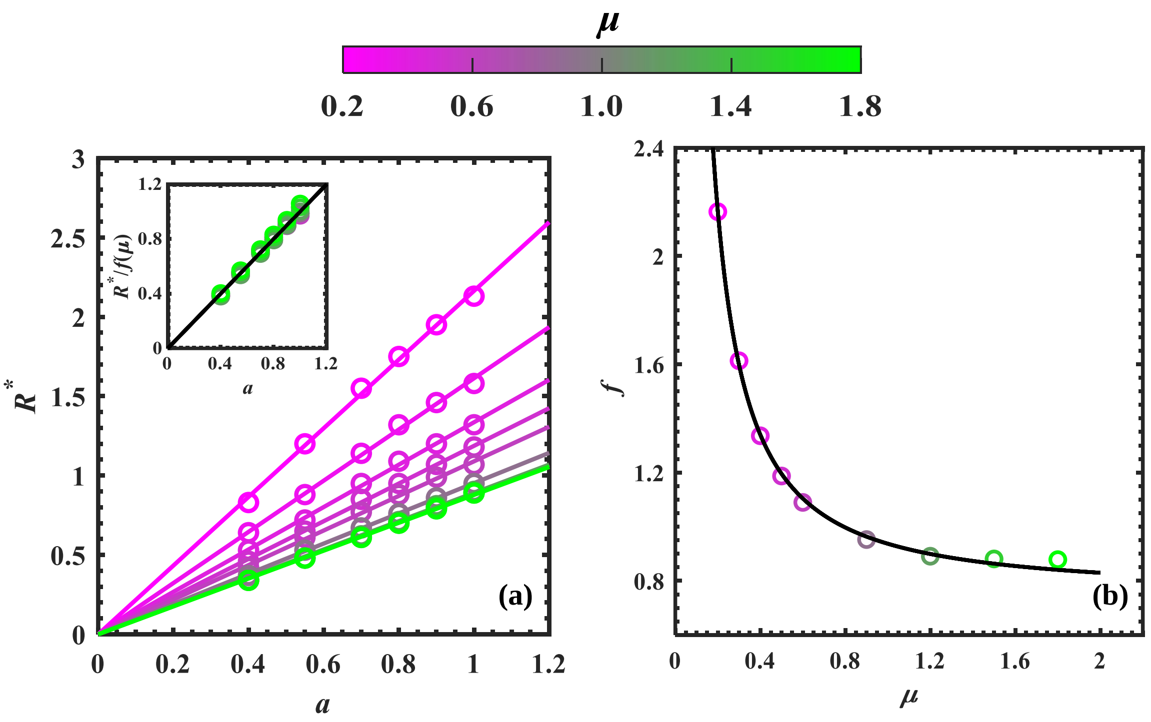

FIG. 5. (a) Evolution of normalised run-out distance R^* with low aspect ratios and the fitting results. (b) Fitting results of f–μ.

TABLE IV. Fitting results for low aspect ratios.

μ	f	R^2
0.2	2.163703	0.996497
0.3	1.612932	0.996517
0.4	1.335783	0.997382
0.5	1.187215	0.998206
0.6	1.08964	0.99676
0.9	0.952388	0.999187
1.2	0.890816	0.997525
1.5	0.880822	0.998204
1.8	0.8781778	0.998513

When $a \geqslant 1.7$, the relation between μ and R^* is assumed as an exponential function such as:

$$R^* = \alpha(\mu) \cdot a^{\beta} \tag{11}$$

where $\alpha(\mu)$ is an unknown function. By fitting our simulation results, we obtain a constant value of β equal to 0.49 in TABLE V. For the function of $\alpha(\mu)$, we use the same approach as for $f(\mu)$

$$\alpha(\mu) = \frac{A}{\mu^{B}} + C \tag{12}$$

where A, B, and C are fitted parameters and are all positive. The fitting results are presented in FIG. 6(b), with the corresponding parameter values of $A = 0.023$, $B = 2.572$, $C = 1.408$, and $R^2 = 0.993$. The linearity of each point, as indicated by the slope ratio of 0.49, is verified by the inset plot of FIG. 6(a) that we plot in logarithmic scale. The same explanation provided for low aspect ratios in term of the influence of μ applies here. Finally, conversely to low aspect ratios, when $\mu \to \infty$, the final run-out distance depends on aspect ratio and $R^* = 1.408a^{0.49}$. The final formula for higher aspect ratios is:

$$R^* = \left(\frac{0.023}{\mu^{2.572}} + 1.408\right) \cdot a^{0.49} \tag{13}$$

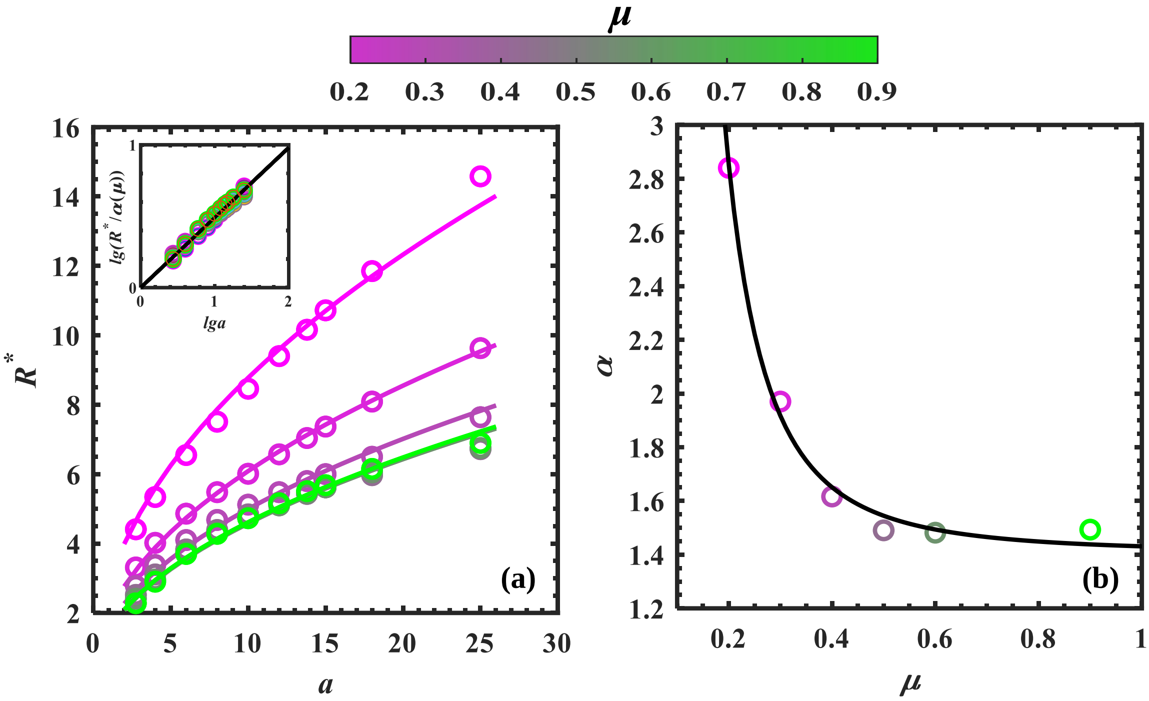

FIG. 6. (a) Evolution of normalised run-out distance with higher aspect ratios in different friction coefficients. (b) Fitting results for higher aspect ratio models.

TABLE V. Fitting results for larger aspect ratios.

μ	α	β	R^2
0.2	2.840004	0.49	0.9861
0.3	1.969984	0.49	0.9978
0.4	1.616418	0.49	0.9883
0.5	1.490427	0.49	0.9666
0.6	1.481723	0.49	0.9822
0.9	1.493148	0.49	0.9888

Equation (14) summarizes the modified formulas for the run-out distance considering the basal friction coefficient. Compared with those in **Error! Reference source not found.**, we find that the frontier factors (f and α) are highly dependent on the basal friction coefficient, while the index parameters (β) are independent of it. Notably, for $a < 1.7$, the index parameter is the same as that proposed by Ref. [1]; and for $a > 1.7$, our result of 0.49 is very close to the result of Ref. [1] of 0.5.

$$\frac{r_\infty - r_0}{r_0} = \begin{cases} \left(\dfrac{0.1834}{\mu^{1.268}} + 0.7536\right) \cdot a, & a < 1.7 \\ \left(\dfrac{0.023}{\mu^{2.572}} + 1.408\right) \cdot a^{0.49}, & a \geq 1.7 \end{cases} \tag{14}$$

B. Final height

The relationship between the rescaled final height, h_∞, and aspect ratio for various friction coefficients can be characterized by three distinct stages shown in FIG. 7. Initially, there is a linear increase stage, followed by an exponential increase stage. Subsequently, a decrease stage occurs. Our results (μ=0.4) are plotted in FIG. 7 and compared to experimental and numerical results as well the proposed formula by Lube, et al. [1] shown in Eq. (15).

$$\frac{h_\infty}{r_0} = \begin{cases} a, & 0 \le a < 1.7 \\ 0.88a^{1/6}, & 1.7 \le a < 10 \end{cases} \tag{15}$$

Our simulations fit well with their experimental results as well as their proposed formula when $a < 10$. They did not provide a relationship for $a > 10$. Yang, et al. [24] carried out analysis for values of $a > 10$ using SPH method. Our results seem to fit the experimental results of Ref. [1] better whilst confirming the trend as Ref. [24]. This allows us to propose a trilinear approximation proposed in Eq. (16). Critically, and in agreement with the results of Ref. [24], the results indicate that for larger values of a, the final height decreases as the aspect ratio increases. We find that the friction coefficient has less effect on the linear increase stage, while it becomes more relevant in the other stages.

The extended forms in this study for axisymmetric granular column collapse with a wide range of aspect ratios are:

$$\frac{h_\infty}{r_0} = \begin{cases} a, & 0 \le a < 0.86 \\ 0.88 \cdot a^{1/6}, & 0.86 \le a < 10 \\ 1.853 \cdot a^{-0.189}, & a \ge 10 \end{cases} \tag{16}$$

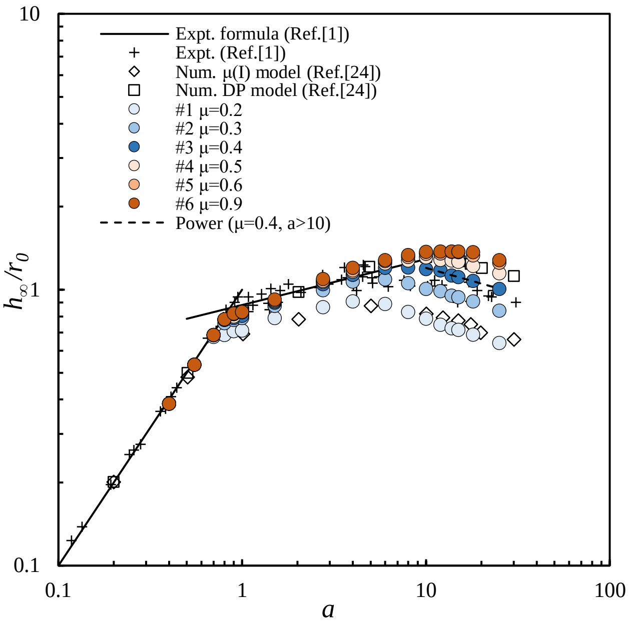

FIG. 7. The relationship between rescaled final height and aspect ratio.

FIG. 8 shows the contour map of rescaled final height projected on a μ-a plane. There are turning points in the contour area for the different colours, marked by the orthogonal points of the black arrow and contour lines, which represent the maximum rescaled final height point for each friction coefficient. It indicates that an increase in the friction coefficient affects the separation point (maximum final height) between the exponential increase stage and the decrease stage, resulting in an increase in the aspect ratio corresponding to the maximum final height. When a<2.5, the effect of μ on the final height is negligible. Conversely, for cases where a>2.5, the final height is influenced by μ. This is the reason why Ref. [2] found that roughness only had influence on the final height of the larger aspect ratio models. It is worth noting that when the friction coefficient exceeds 0.5, there is a red trapezoidal zone (maximum h_∞/r_0=1.3-1.4 as shown in FIG. 8), which is due to the redundancy of the friction at the substrate, where the effect of friction on the final height converges into a single value. This non-linear relationship between the friction coefficient and maximum height highlights the complexity of particle dynamics and the need for careful consideration of multiple factors when evaluating particle behaviour.

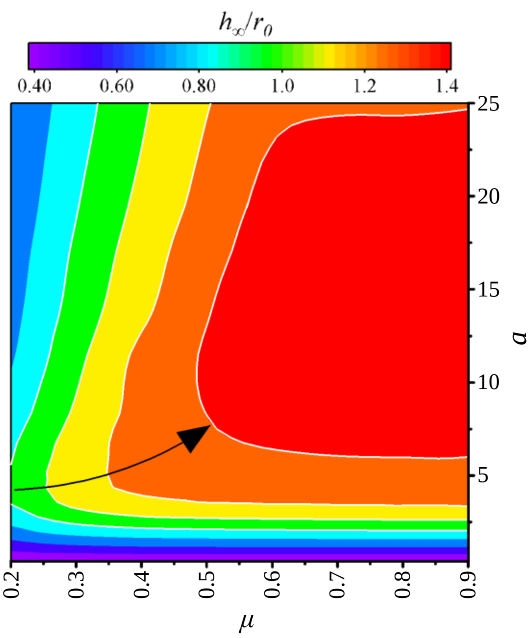

FIG. 8. Contour map of rescaled final height projected on μ-a plane.

C. Deposit morphology

Granular columns collapse to form different morphology, primarily depending on their initial aspect ratio. All final deposit morphologies can be classified by three regimes [1, 2, 19]:

(1) Regime I: the granular materials spread through the avalanche on its flank and produces a circular undisturbed area at the upper surface of the column, forming a circular truncated cone, e.g., the flow pattern with a=0.55 at t/t_{max}=0.8-1.0 as shown in FIG. 3;

(2) Regime II: the entire upper surface starts to flow immediately, forming a tip with a cone-like shape, e.g., the flow pattern with a=2.75 at t/t_{max}=0.8-1.0 as shown in FIG. 3;

(3) Regime III: a concentric wave originates and propagates outwards, e.g., the flow pattern with a=13.8 at t/t_{max}=0.8-1.0 as shown in FIG. 3. The final shape has been named differently by other researchers: 'Mexican hat' for a>3 [2], liquid-like [19].

The regime identification process from the numerical models is illustrated in Appendix B.

The results of deposit regime for all the models are shown in FIG. 9, with each regime type represented by a different colour. The results show that the basal friction clearly influences the deposit regime. Two transition zones are revealed (indicated by dashed blue lines). Contrary to what was stated in previous studies, these depend on competition mechanism between the initial column aspect ratio and basal friction coefficient. The first transition (Zone 1 in the figure) between regime I to regime II, occurs for when the friction coefficient varies from 0.1 to 0.2 and the aspect ratios between 0.5 and 0.8. Zone 2 (regime II to III) is defined by values of friction coefficient between 0.3 to 0.7 and aspect ratios from 8 to 25. Since Ref. [19] does not consider the extreme conditions (zero and +∞) of the particle-boundary friction, their results only show one transition zone at μ>0.1.

These findings provide an explanation to the results reported by Ref. [3], who showed that friction force dominates flow behaviour for small aspect ratios, without quantifying it fully. For models with medium aspect ratios (0.7<a<6), regime II is the sole regime observed, indicating that although basal friction continues to play a role, it is gradually replaced by pressure gradient effects. This is the reason why Ref. [16] found no influence of basal friction as they used a = 1.91. When the aspect ratio exceeds 6, a second transition zone emerges. Within this range, as the friction coefficient increases from 0.7 to 0.3 (as indicated by the direction of the black arrows), the deposit regime undergoes a transition from regime II to regime III. Finally, as the aspect ratio becomes sufficiently large, the influence of the friction coefficient decreases, and the pressure gradient effects become predominant and all morphologies correspond to regime III. These findings are consistent with those reported by Ref. [3], who demonstrated that for large aspect ratios, flow behaviour is dominated by pressure gradient effects, not the basal friction coefficient.

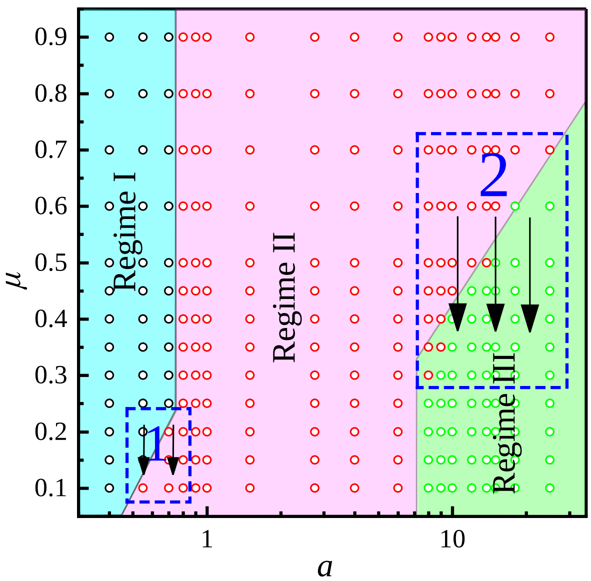

FIG. 9. The results of deposit regimes vary with changes in basal friction coefficients and initial aspect ratios. Blue area: regime I, pink area: regime II, and blue area regime III; Two transition zones (blue dash zones 1 and 2); SPH results (black, red, and green circle points indicate regime I, regime II, and regime III, respectively).

IV. CONCLUSIONS

In this study, we have used SPH to systematically analyse the effects of basal friction on gravity-driven particle column collapse. An SPH model validated against experiments has revealed the following findings:

(1) Run-out distance, final deposit height, and final deposit morphology are all affected by the basal friction.

(2) To predict the run-out distance, we propose a modified formula ($R^* = \alpha \cdot a^{\beta}$) that incorporates the basal friction coefficient μ. Our analysis reveals that μ has an obvious effect on the coefficient factor α in the formula while the exponent parameter β remains unaffected. This model shows two extreme conditions: for $\mu = 0$, the collapsed grains would never stop and thus $R^* \to \infty$; while for $\mu \to \infty$, every grain would become quiescent at all times as soon as it touches the substrate, under which the column can be deemed collapsed onto one layer of its composed grains. That is to say, the influence of basal friction converges to that of grain friction. Somewhat surprisingly, for low aspect ratio models, the minimum run-out distance increases linearly as the aspect ratio increases, with a slope of 0.7536. And this value is equal to the *tan* value of the internal friction angle (*tan* 37°=0.7536) of the material. This means the minimum run-out distance depends on the material internal friction angle.

(3) The basal friction also exerts an influence on the final height, with higher friction coefficients resulting in greater final heights. The relationship between the rescaled final height and aspect ratio in

the same friction coefficient models can be characterized by three distinct stages: linear increase stage; exponential increase stage; and decrease stage. The friction coefficient has little influence in the linear increase stage, while it becomes more relevant in the other stages. Specifically, an increase in the friction coefficient affects the separation point (maximum final height) between the exponential increase stage and the decrease stage, resulting in an increase in the aspect ratio corresponding to the maximum final height. However, we observe a convergence of the effect of basal friction on the final height when $\mu > 0.5$.

(4) The basal friction also affects the deposit regime. The competition mechanism between the initial column aspect ratio and basal friction coefficient reveals two transition zones that delimit the three main deposit regimes reported in the literature. In zone 1 (regime I to regime II), the friction coefficient varies from 0.1 to 0.2 and the aspect ratios between 0.5 and 0.8. Zone 2 (regime II to III) is defined by values of friction coefficient between 0.3 to 0.7 and aspect ratios from 8 to 25.

ACKNOWLEDGEMENTS

The author acknowledges the financial support of China Scholarship Council.

APPENDIX A: SPH ARTIFICIAL VISCOSITY

The concept of artificial viscosity was first proposed in one spatial dimension by Ref. [29] to model flows with shocks, which is nowadays widely used in wave propagation programs. The role of the artificial viscosity is to smooth the shock over several particles. The artificial viscosity term Π_{ij} [30] is included in the SPH momentum equation as:

$$\frac{d\boldsymbol{v}_i}{dt} = \sum_{j\in P} m_j \left(\frac{\boldsymbol{\sigma}_i}{\rho_i^2} + \frac{\boldsymbol{\sigma}_j}{\rho_j^2} + \Pi_{ij}\mathbf{I} \right) \nabla W_{ij} + \boldsymbol{b}_i \tag{A1}$$

where **I** is the identity matrix. The most widely used form of artificial viscosity is:

$$\Pi_{ij} = \begin{cases} \dfrac{-\alpha c_{ij}\phi_{ij} + \beta\phi_{ij}^2}{\rho_{ij}}, & u_{ij}\cdot x_{ij} < 0 \\ 0, & u_{ij}\cdot x_{ij} \gg 0 \end{cases} \tag{A2}$$

$$\phi_{ij} = \frac{h_{ij}\boldsymbol{v}_{ij}\cdot\boldsymbol{x}_{ij}}{\left|\boldsymbol{x}_{ij}^2\right| + 0.01h_{ij}^2},\ c_{ij} = \frac{c_i + c_j}{2}\ ,\ \rho_{ij} = \frac{\rho_i + \rho_j}{2}, \tag{A3}$$

$$h_{ij} = \frac{h_i + h_j}{2}, \boldsymbol{x}_{ij} = \boldsymbol{x}_i - \boldsymbol{x}_j, \boldsymbol{v}_{ij} = \boldsymbol{v}_i - \boldsymbol{v}_j, \tag{A4}$$

where α and β are the problem dependent tuning parameters, and c is the sound speed.

APPENDIX B: MORPHOLOGY DETECTION METHOD

FIG.10shows the method we followed to determine the morphology or deposit regime from our numerical results. For cases where the deposit morphology remains at the initial height with a flat surface at the top, the regime is classified as regime I (e.g., red area in FIG.10, *a*=0.55, μ =0.4). However, if the deposit final height deviates from the initial height, it is classified as either regime II or regime III. For the distinction between regime II and regime III, we inspect the presence of a "double peak". If the morphological image exhibits a continuous colour transition from warm to cold colours, it is categorized as regime II (e.g., *a*=9, μ =0.35, shown in FIG.10) as only one peak at the centre occurs. Conversely, if there is a discontinuous colour transition with the presence of a ring area (second peak), it is classified as regime III (e.g., *a*=9, μ =0.3, shown in FIG.10). This method is highly sensitive, allowing even small differences between regime II and regime III to be detected.

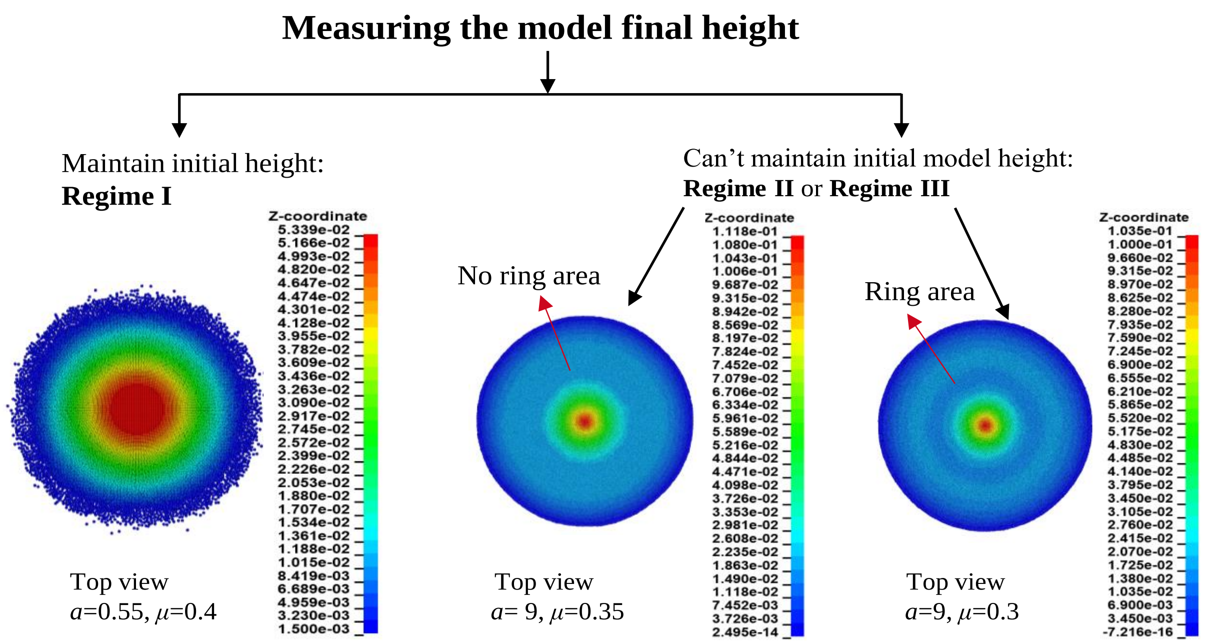

FIG.10. Methodology for determining the deposit regime in LS-DYNA.

References

[1].G. Lube, H.E. Huppert, R.S.J. Sparks and M.A. Hallworth, Axisymmetric collapses of granular columns, Journal of Fluid Mechanics. 508, 175-199 (2004)

[2].E. Lajeunesse, A. Mangeney-Castelnau and J.P. Vilotte, Spreading of a granular mass on a horizontal plane, Physics of Fluids. 16, 2371-2381 (2004)

[3].E. Lajeunesse, J.B. Monnier and G.M. Homsy, Granular slumping on a horizontal surface, Physics of Fluids. 17, 103302 (2005)

[4].N.J. Balmforth and R.R. Kerswell, Granular collapse in two dimensions, Journal of Fluid Mechanics. 538, (2005)

[5].L. Staron and E.J. Hinch, The spreading of a granular mass: role of grain properties and initial conditions, Granular Matter. 9, 205-217 (2006)

[6].E.L. Thompson and H.E. Huppert, Granular column collapses: further experimental results, Journal of Fluid Mechanics. 575, 177-186 (2007)

[7].O. Polanía, M. Cabrera, M. Renouf and E. Azéma, Collapse of dry and immersed polydisperse granular columns: A unified runout description, Physical Review Fluids. 7, 084304 (2022)

[8].G.B. Crosta, S. Imposimato and D. Roddeman, Numerical modeling of 2-D granular step collapse on erodible and nonerodible surface, Journal of Geophysical Research. 114, (2009)

[9].A. Mangeney, O. Roche, O. Hungr, N. Mangold, G. Faccanoni and A. Lucas, Erosion and mobility in granular collapse over sloping beds, Journal of Geophysical Research. 115, (2010)

[10].M. Cabrera and N. Estrada, Granular column collapse: Analysis of grain-size effects, Phys Rev E. 99, 012905 (2019)

[11].T. Man, H.E. Huppert, L. Li and S.A. Galindo‐Torres, Finite‐Size Analysis of the Collapse of Dry Granular Columns, Geophysical Research Letters. 48, (2021)

[12].L. Jing, C.Y. Kwok, Y.F. Leung, Z. Zhang and L. Dai, Runout Scaling and Deposit Morphology of Rapid Mudflows, Journal of Geophysical Research: Earth Surface. 123, 2004-2023 (2018)

[13].R. Zhu, Z. He, K. Zhao, B. Vowinckel and E. Meiburg, Grain-resolving simulations of submerged cohesive granular collapse, Journal of Fluid Mechanics. 942, (2022)

[14].C. Goujon, N. Thomas and B. Dalloz-Dubrujeaud, Monodisperse dry granular flows on inclined planes: role of roughness, Eur Phys J E Soft Matter. 11, 147-157 (2003)

[15].O. Roche, M. Attali, A. Mangeney and A. Lucas, On the run-out distance of geophysical gravitational flows: Insight from fluidized granular collapse experiments, Earth and Planetary Science Letters. 311, 375-385 (2011)

[16].C. Frank, Three-Dimensional Discrete Element Simulation of Axi-symmetric Collapses of Granular Columns, Engineering Computations. (2006)

[17].X. Zhang, Y. Ding, D. Sheng, S.W. Sloan and W. Huang, Quasi-static collapse of two-dimensional granular columns: insight from continuum modelling, Granular Matter. 18, (2016)

[18].B. Sheikh, T. Qiu and A. Ahmadipur, Comparison of SPH boundary approaches in simulating frictional soil–structure interaction, Acta Geotechnica. 16, 2389-2408 (2021)

[19].T. Man, H.E. Huppert, L. Li and S.A. Galindo-Torres, Deposition morphology of granular column collapses, Granular Matter. 23, (2021)

[20].W. Chen and T. Qiu, Numerical Simulations for Large Deformation of Granular Materials Using Smoothed Particle Hydrodynamics Method, International Journal of Geomechanics. 12, 127-135 (2012)

[21].K. Szewc, Smoothed particle hydrodynamics modeling of granular column collapse, Granular Matter. 19, (2017)

[22].N. Fávero, Alomir H. and R.I. Borja, Continuum hydrodynamics of dry granular flows employing multiplicative elastoplasticity, Acta Geotechnica. 13, 1027-1040 (2018)

[23].E. Kermani and T. Qiu, Simulation of quasi-static axisymmetric collapse of granular columns using smoothed particle hydrodynamics and discrete element methods, Acta Geotechnica. 15, 423-437 (2018)

[24].E. Yang, H.H. Bui, H. De Sterck, G.D. Nguyen and A. Bouazza, A scalable parallel computing SPH framework for predictions of geophysical granular flows, Computers and Geotechnics. 121, (2020)

[25].H.H. Bui and G.D. Nguyen, Smoothed particle hydrodynamics (SPH) and its applications in geomechanics: From solid fracture to granular behaviour and multiphase flows in porous media, Computers and Geotechnics. 138, (2021)

[26].J.O. Hallquist, LS-DYNA® Theory Manual. Livermore Software Technology Corporation, Livermore, California (2006)

[27].E. Kermani and T. Qiu, Simulation of Quasi-Static and Dynamic Collapses of Rectangular Granular Columns Using Smoothed Particle Hydrodynamics Method, International Journal of Geomechanics. 18, (2018)

[28].C. Peng, S. Wang, W. Wu, H.-S. Yu, C. Wang and J.-Y. Chen, LOQUAT: an open-source GPU-accelerated SPH solver for geotechnical modeling, Acta Geotechnica. 14, 1269-1287 (2019)

[29].J. Vonneumann and R.D. Richtmyer, A Method for the Numerical Calculation of Hydrodynamic Shocks, Journal of Applied Physics. 21, 232-237 (1950)

[30].Monaghan and R.A. Gingold, Shock Simulation by the Particle Method of SPH, Journal of Computational Physics. 52, 374-389 (1983)